Two-Pump Optical Manipulation of Resonant Spin Amplification

Estefanio Kesto, ^{1, a)} Michael J. Dominguez, ¹ and Vanessa Sih¹ Department of Physics, University of Michigan, Ann Arbor, Michigan 48109, USA

(Dated: 28 April 2023)

An experimental and computational optical pump-probe model is constructed which utilizes two ultrafast pump pulses within the repetition period of a mode-locked laser to generate electron spin polarization. This report focuses on the effects of resonant spin amplification induced by an infinite train of the two pump pulses. One pump pulse is used to generate ordinary resonant spin amplification spectra while the second pump pulse is used to manipulate the generated spectra. This model gives control of the accumulation of spin polarized electrons along a magnetic field by selecting the temporal separation of the two pump pulses. The computational model accurately predicts and agrees with the experimental results which shows manipulation of resonant spin peaks that are no longer entirely dependent on the external magnetic field. This two-pump model and the associated manipulations of resonant spin peaks can be used as a platform to construct and conceptualize resonant spin amplification-based optospintronic devices and applications.

I. INTRODUCTION

Ultrafast optical pump-probe techniques are used to generate spin polarized electrons while time and magnetic field-resolved Kerr or Faraday rotation measurements provide insight into the respective spin dynamics¹⁻⁴. Both measurement techniques involve measuring the rotation variation in the polarization plane of linearly polarized light. The differences in the two measurement techniques is that measuring the magneto-optic Kerr and Faraday effect allow one to measure the rotation variation of the polarization plane for reflection and transmission of linearly polarized light, respectively. The former technique is generally used for nontransparent samples while the latter is generally used for transparent samples.

In the optical pump-probe technique utilized in this investigation, an optical pump is circularly polarized to generate spin polarized electrons, and an optical probe is linearly polarized to detect and quantify the spin polarization. There is a multifold increase in the spin accumulation and sharp magnetic field-dependent resonances when the spin polarization is excited by an infinite train of ultrafast laser pulses that arrive at time intervals shorter than or on the order of the spin lifetime¹. More specifically, these resonances occur when the consecutive generation of electron spin polarization are in phase with the Larmor precession frequency of the electron spin^{1,3,5}.

The Larmor frequency is defined by $\Omega = \mu_B B_{ext} g/\hbar$, where μ_B is the Bohr magneton, B_{ext} is the externally applied magnetic field, g is the electron g factor, and \hbar is the reduced Planck's constant. The resonance condition occurs when an integer multiple of the Larmor period $(n2\pi/\Omega)$ equals the repetition period of the mode-locked laser (T_{rep}) . Sharp field-dependent peaks therefore occur every $B_n = n2\pi\hbar/\mu_B T_{rep} g$, where n is an integer (n = 0, 1, 2, ...) and B_n is known as the phase synchronization condition (PSC). This type of spin resonance is known as resonant spin amplification (RSA)¹ and also occurs in the spin mode locking (SML) effect^{6,7}.

Although RSA and SML correspond to the same phenomena – sharp periodic magnetic field-dependent peaks – they are a consequence of two different manifestations⁶. The dif-

ferent manifestations are a result of two variables: (1) the degree of homogeneity of the corresponding spin ensembles and (2) excitation pump powers. The RSA/SML manifestations correspond to sufficiently small/large inhomogeneity and small/large excitation pump powers.^{6,7}.

The technique of RSA and SML has been extensively used to investigate the spin dynamics within bulk semiconductors^{1,3,5,8–11}, quantum dots^{7,12}, and II-VI and III-V quantum wells^{13–16}. RSA and SML spectra allow individuals to quantify information regarding spin dynamics due to the insight it gives into the respective systems' spin dephasing (i.e., spin lifetime)^{1,17}, g factor^{10,18}, decoherence properties¹⁹, and the coupling of electron spins to nuclear spins^{3,9,12,13}.

Experiments employing the optical pump-probe technique utilizing two pump pulses have conceptualized optomagnonic logic devices²⁰ and have investigated spin dynamics which are present within direct band-gap semiconductor, ferrimagnetic, and antiferrimagnetic materials (see H. Shibata et al.²¹ and references therein). An RSA-based two-pump study has been employed to more accurately interpret electron spin lifetime¹⁷. Two-pump investigations regarding spin polarized electrons have demonstrated control in spin coherence²² as well as spin tipping/rotating on timescales shorter than the spin coherence time – all while preserving spin coherence – which provides a pathway to perform many single qubit operations within the spin coherence time $^{23-25}$. The subject of this report focuses on the manipulation of RSA spectra induced in an optical pump-probe model which utilizes an infinite train of two pump pulses that are within the repetition period of the mode-locked laser and temporally separated from each other.

The experimental and computational model allows one to choose where in the Larmor precession the optical rotation occurs about a magnetic field. This results in the selective rotation of electron spins which shows further control and manipulation of RSA peaks that are no longer entirely dependent on the externally applied magnetic field. The model accurately predicts the expected RSA peaks for Kerr or Faraday rotation measurements for any given externally applied magnetic field, pump-pump temporal separations, pump-probe time delay, and pump polarizations. Manifestations of RSA induced by this two-pump model can be used to investigate and characterize applications toward RSA-based optospintronic devices.

a) Electronic mail: ekesto@umich.edu

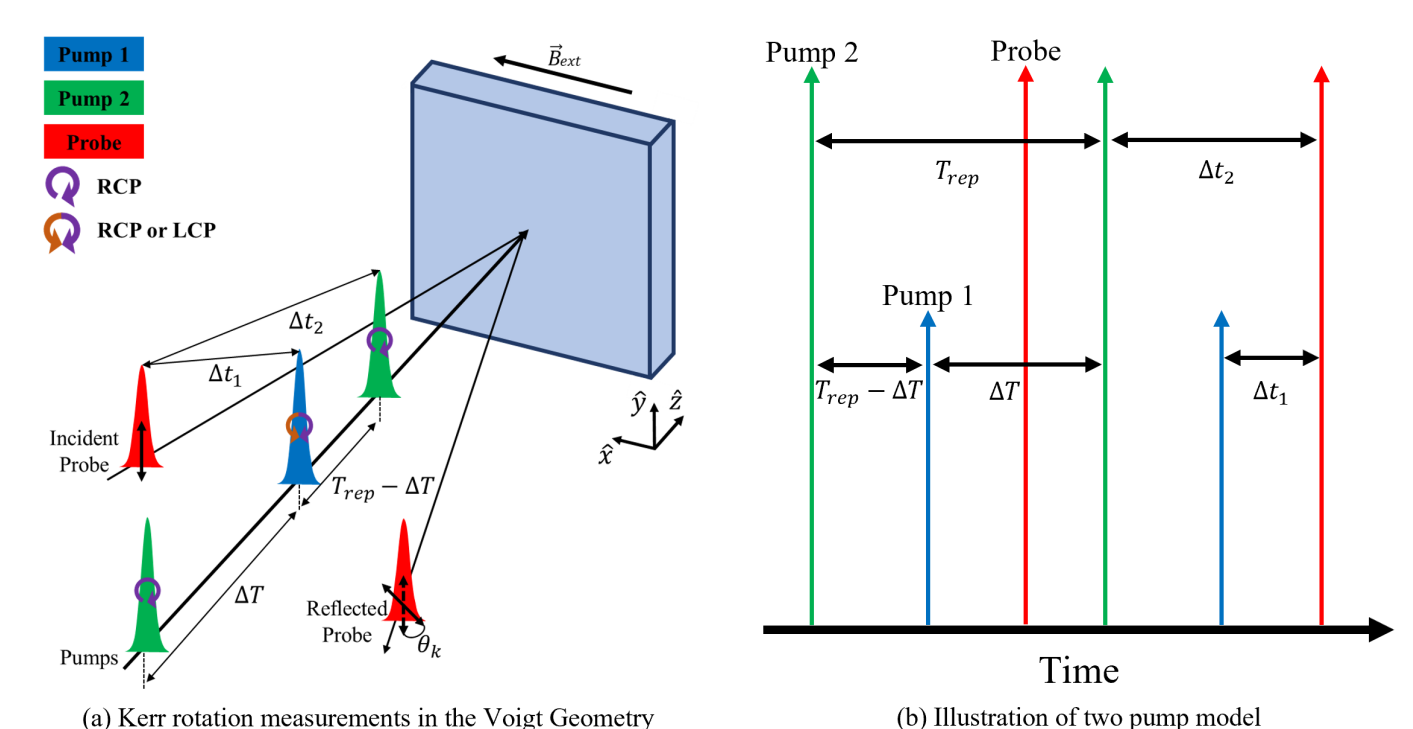


FIG. 1: Two pump schematic. (a) Two pump pulses generate spin polarization along the z-axis. Pump 2 is denoted as the generator as it is used to generate ordinary RSA spectra. Additionally, Pump 2 is right circularly polarized (RCP) and has a pump-probe delay of Δt_2 for all the measurements presented hereafter. Pump 1 is denoted as the manipulator as it used to manipulate the ordinary RSA spectra generated by Pump 2. Pump 1 may have its polarization helicity chosen to either be left circularly polarized (LCP) or RCP and its pump-probe delay (Δt_1) may be arbitrarily set. A linearly polarized probe beam detects the spin polarization component along the z-axis by measuring the change in the plane of polarization after reflection (i.e., the Kerr rotation θ_k). (b) Train of two pump pulses followed by a probe pulse. Pump 1, Pump 2, and the probe all have a repetition period of T_{rep} with respect to themselves. The two pumps have time separations of Δt_1 and Δt_2 with respect to the probe and two time separations of ΔT and $T_{rep}-\Delta T$ with respect to each other where $\Delta T = \Delta t_1 + (T_{rep}-\Delta t_2)$.

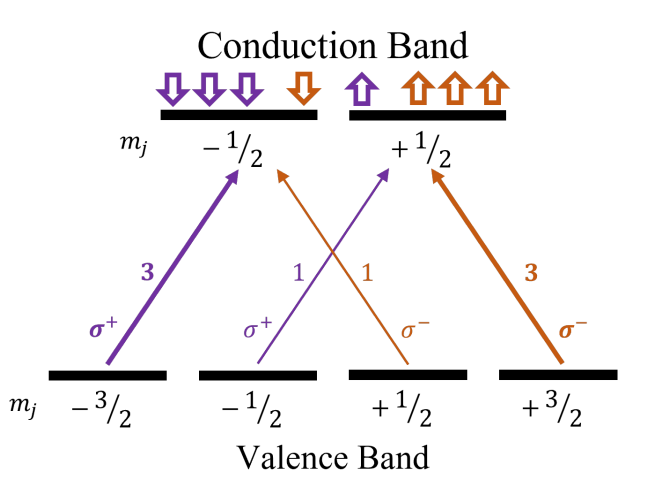


FIG. 2: Depiction of optically excited spin-up and spin-down conduction band filling in GaAs. The spin-up and spin-down excitations correspond to the $+^1/_2$ and $-^1/_2$ in the conduction band, respectively. The convention used in this report take σ^+/σ^- as right/left handed circular polarizations.

II. TWO-PUMP MODEL

A. Role of Pump Polarization

In Fig. 1, Pump 2 acts as the RSA generator with a constant pump-probe delay of Δt_2 and therefore its polarization is configured to have a constant right handed circular polarization throughout these investigations. Pump 1 is considered the RSA manipulator and its polarization may be configured to be either right or left circularly polarized. The convention of denoting Pump 2 as the generator and Pump 1 as the manipulator is due to the roles Pump 2 and Pump 1 take part in this model – Pump 2 is used to generate ordinary RSA spectra and Pump 1 is used to manipulate the ordinary RSA spectra generated by Pump 2.

This report utilizes optical spin orientation to establish spin polarized electrons in a bulk n-doped GaAs sample because of the role polarization helicity takes part in the generation of spin polarization. Optical selection rules govern the transitional probabilities between the valence and conduction band states upon the sample absorbing either RCP or LCP light. In-depth discussion on optical spin orientation and selection rules for GaAs can be found in Ref. 24.

The optical selection rules and corresponding convention used here result in RCP light exciting 1 spin-up and 3 spin-down electrons and, conversely, LCP light will excite 3 spin-

up and 1 spin-down (Fig. 2). This gives rise to a non-zero difference of optically excited spin-up to spin-down states which results in spin polarization of the dominant spin type. In other words, RCP/LCP will generate spin polarization of the spin-down/up type along the optical axis. Relating $\sigma^{+/-}$ to right or left circular polarization is solely based on convention; the convention used here correspond σ^+ and σ^- to RCP and LCP light, respectively.

B. Theoretical Model

In this two pump model, the dynamics of RSA are generated and studied using the magnetic field-resolved Kerr rotation (FRKR) optical pump-probe technique in the Voigt geometry. The experiments are performed such that circularly polarized light propagates and generates spin polarized electrons along the z-axis (i.e., the optical axis). An external magnetic field with a magnitude of B_{ext} is applied perpendicular to the optical axis along the x-direction (Fig. 1a). The spin polarized electrons thereby precess about the magnetic field axis and are classically described by

$$S_x(t) = S_{0x} e^{-t/T_2^*} (1)$$

$$S_{y}(t) = -\frac{1}{2} S_{0} sin(\Omega t) e^{-t/T_{2}^{*}}$$
 (2)

$$S_z(t) = ^+_- S_0 cos(\Omega t) e^{-t/T_2^*}$$
 (3)

where Ω is the Larmor precession frequency as defined in the introduction, T_2^* is the electron spin lifetime, S_0 is the spin polarization generated along the z-direction, and S_{0x} is the spin component of the spin polarization along the x-direction. The model presented here takes the g-factor as g=-0.44 and spin lifetime as $T_2^*=15$ ns. Additionally, this model assumes the spin lifetime and g-factor for each spin component are isotropic and homogeneous (i.e., $g_x=g_y=g_z=g$ and $T_{2x}^*=T_{2y}^*=T_{2z}^*=T_2^*$). It is important to note that Eqs. 1, 2, and 3 describe the spin precession of polarized electrons for a single laser pulse.

Relations may be deduced between the spin components pre(-) and post(+) pump pulses when the pulse duration is much less than the repetition period of the laser. Additionally, $S_x(t) = 0$ on resonance. To generalize the pre(-)/post(+) relations, it is convenient to implement a rotational matrix about the x-axis for the Larmor precession $R_{\Omega}(t)$ and a spin generation vector \overrightarrow{G} .

$$R_{\Omega}(t) = \begin{bmatrix} 1 & 0 & 0\\ 0 & cos(\Omega t) & -sin(\Omega t)\\ 0 & sin(\Omega t) & cos(\Omega t) \end{bmatrix}$$
(4)

$$\overrightarrow{G} = \begin{bmatrix} 0 \\ 0 \\ -S_0 \end{bmatrix}$$
 (5)

The +/- sign in the spin generation vector \overrightarrow{G} correspond to LCP/RCP pump polarization. This sign convention is chosen because LCP and RCP pumps generate spin polarization of the spin-up and spin-down type, respectively. Additionally, the spin decay e^{-t/T_2^*} may be taken to be constant because

the assumption of T_2^* being isotropic and homogeneous. The generalized spin vector $\overrightarrow{S}(t)$ using these relations become

$$\begin{bmatrix} S_x(t) \\ S_y(t) \\ S_z(t) \end{bmatrix} = \begin{bmatrix} 1 & 0 & 0 \\ 0 & \cos(\Omega t) & -\sin(\Omega t) \\ 0 & \sin(\Omega t) & \cos(\Omega t) \end{bmatrix} \begin{bmatrix} 0 \\ 0 \\ -S_0 \end{bmatrix} e^{-t/T_2^*}$$
(6)

$$\overrightarrow{S}(t) = R_{\Omega}(t) \overrightarrow{G} e^{-t/T_2^*} \tag{7}$$

With this notation, the first pump pulse generates the spin vector \overrightarrow{G} at time t=0. Then, for the duration $0 < t < T_{rep}$ prior to the next pump pulse, the spins precess and decay by $R_{\Omega}(t)$ and e^{-t/T_2^*} , respectively. At the time directly following the next pump pulse $(t=T_{rep}^+)$ the relation $\overrightarrow{S}^+ = \overrightarrow{S}^-$ is invoked where $\overrightarrow{S}^- = \overrightarrow{S}(T_{rep})$. The next set of generated spins are added to this relation giving

$$\overrightarrow{S}(t = T_{rep}^{+}) = R_{\Omega}(T_{rep}) \overrightarrow{G} e^{-T_{rep}/T_{2}^{*}} + \overrightarrow{G}$$
 (8)

This is repeated for an infinite train of single pump pulses, followed by single probe pulses temporally separated by the laser repetition period T_{rep} , which results in an infinite summation that geometrically converges and has the form

$$\overrightarrow{S}_{one}^{+}|_{\infty} = \left[\sum_{n=0}^{\infty} \left(R_{\Omega}(T_{rep})e^{-T_{rep}/T_{2}^{*}}\right)^{n}\right] \overrightarrow{G}$$

$$= \left[\mathbb{1} - R_{\Omega}(T_{rep})e^{-T_{rep}/T_{2}^{*}}\right]^{-1} \overrightarrow{G}$$
(9)

where 1 is a 3 x 3 identity matrix and $\overrightarrow{S}_{one}^+|_{\infty}$ represents the spin accumulation for a single-pump single-probe model. The convergent form of Eq. 9 would result in FRKR experimental measurements with a pump-probe delay of $\Delta t = 0$. Applying the Larmor precession $R_{\Omega}(\Delta t)$ and spin decay $e^{-\Delta t/T_2^+}$ to Eq. 9 gives

$$\overrightarrow{S}(\Delta t) = R_{\Omega}(\Delta t)e^{-\Delta t/T_2^*} \left[\overrightarrow{S}^+|_{\infty}\right]$$
 (10)

where $\overrightarrow{S}^+|_{\infty}$ is the spin accumulation for an infinite train of pump pulses and $\overrightarrow{S}(\Delta t)$ is the corresponding total spin vector valid any arbitrary pump-probe time delay that is valid for $0 < \Delta t < T_{rep}$.

The summation and closed form solution of Eq. 9 are only valid for the case where the spin vector follows the pattern of spin polarization generation \rightarrow precession/decay \rightarrow detection. In other words, a single pump pulse is used to generate spin polarization, the polarized electrons precess and decay with time, then a single probe pulse detects the spin vector. Modifications must be made to Eq. 9 for a scheme which utilizes two pump pulses followed by a single probe pulse because the spin vector for a two pump scheme follows the pattern of spin polarization generation \rightarrow precession/decay \rightarrow spin polarization generation \rightarrow precession/decay \rightarrow detection²⁷. This two pump scheme has a different spin vector pattern when comparing it to the pattern of the single pump scheme; the two/single pump have 2/1 iteration(s) of spin polarization generation \rightarrow precession/decay before the probe pulse detects the resulting spin vector.

In the model presented here, there are two pump pulses within the repetition period of the probe pulse and therefore there are two time scales of interest - the time scales of interest being ΔT and $T_{rep} - \Delta T$ (Fig. 1b). Two new matrices are introduced to account for the spin polarization generation and Larmor precession/decay from the second pump pulse. This results in a total of five matrices for the two pump model rather than three matrices used for the one pump model. The five matrices of interest are $R_{\Omega}(\Delta T)$, $R_{\Omega}(T_{rep} - \Delta T)$, $R_{\Omega}(\Delta t)$, \overrightarrow{G}' , and \overrightarrow{G} , where \overrightarrow{G}' and \overrightarrow{G} correspond to the spin polarization generated from Pump 1 and Pump 2, respectively. By introducing these respective matrices, the model now accounts for the two pump pulses having temporal separations of ΔT and $T_{rep} - \Delta T$, followed by a probe pulse with a temporal separation from its nearest pump pulse neighbor upon detection of Δt (Fig. 1b). According to Fig. 1b, Pump 1 is the nearest neighbor to the probe upon detection and Δt_1 is the corresponding

The spin dynamics for the two pump model may now be properly described. Following the procedure to get the corresponding $\overrightarrow{S}^+|_{\infty}$, but now for an infinite train of two pump pulses, $\overrightarrow{S}^+|_{\infty}$ takes the new form

pump-probe delay.

$$\begin{split} \overrightarrow{S}_{two}^{+}|_{\infty} &= \left[\sum_{n=0}^{\infty} \left(R_{\Omega}(T_{rep} - \Delta T)R_{\Omega}(\Delta T)e^{-T_{rep}/T_{2}^{*}}\right)^{n}\right] \overrightarrow{G}' + \\ &\left(R_{\Omega}(T_{rep} - \Delta T)e^{-(T_{rep} - \Delta T)/T_{2}^{*}}\right) * \\ &\left[\sum_{n=0}^{\infty} \left(R_{\Omega}(\Delta T)R_{\Omega}(T_{rep} - \Delta T)e^{-T_{rep}/T_{2}^{*}}\right)^{n}\right] \overrightarrow{G}' + \\ &= \left[\mathbb{1} - R_{\Omega}(T_{rep} - \Delta T)R_{\Omega}(\Delta T)e^{-T_{rep}/T_{2}^{*}}\right]^{-1} \overrightarrow{G}' + \\ &\left(R_{\Omega}(T_{rep} - \Delta T)e^{-(T_{rep} - \Delta T)/T_{2}^{*}}\right) * \\ &\left[\mathbb{1} - R_{\Omega}(\Delta T)R_{\Omega}(T_{rep} - \Delta T)e^{-T_{rep}/T_{2}^{*}}\right]^{-1} \overrightarrow{G}' + \\ \end{split}$$

where $\overrightarrow{S}_{two}^+|_{\infty}$ represents the spin accumulation from a double-pump single-probe model and \overrightarrow{G}' as well as \overrightarrow{G} must follow the +/- sign convention for either LCP/RCP pump polarizations. Eq. 11 corresponds to the probe pulse having a temporal separation to its nearest neighbor pump pulse of $\Delta t = 0$. Multiplying Eq. 11 by $R_{\Omega}(\Delta t)$ and $e^{-\Delta t/T_2^*}$ gives Eq. 10, which results in the total spin vector $\overline{S}(\Delta t)$ for any arbitrary pump-probe delay valid for $0 < \Delta t < \Delta T_{max}$, where Δt and ΔT_{max} correspond to the probes nearest neighboring pump pulse (Δt_1 in Fig. 1b) and the maximum pump-pump temporal separation allowed by the experimental set up, respectively. The expected RSA peaks for FRKR experiments utilizing two pumps followed by a single probe are now able to be calculated and plotted for any given externally applied magnetic field (B_{ext}), pump-pump temporal separations (ΔT and $T_{rep} - \Delta T$), nearest pump-probe time delay upon probe detection (Δt_1), and pump polarizations.

Carrying out the involved matrix multiplication for Eq. 10

results in a cumbersome end equation. Groups have worked to significantly simplify Eq. 10 and there exists different closed forms of Eq. 10 which are functionally equivalent. The functionally equivalent different forms of Eq. 10 come from phasor, trigonometric, or algebraic manipulations to put the total spin vector in a form with variables that carry physical significances^{28–30}. The resulting total spin vector used in this report for the one- and two-pump regimes are Eq. A1 and Eq. A2, respectively, which can be found in the appendix.

C. Experimental Model

The spin dynamics investigated here are conducted on a $2-\mu$ m-thick active GaAs epilayer with a Si-doped density of $n=3*10^{16}cm^{-3}$. The active GaAs layer is grown on a 1- μ m-thick inactive undoped AlGaAs layer and the AlGaAs is grown on an inactive undoped (001)-oriented GaAs substrate where both the active GaAs and inactive AlGaAs are grown by molecular-beam epitaxy. The sample is mounted in a helium flow cryostat maintained at a nominal temperature of 10K and placed in between the poles of an electromagnet.

A mode-locked Ti:S laser source tuned near the band gap of the active GaAs is configured to output \sim 2 ps pulses at a repetition rate of 76 MHz which corresponds to a repetition period (T_{rep}) of 13.16 ns. This source is used to both generate and detect the spin dynamics through degenerate pump-probe (i.e., pump and probe are of the same wavelength) FRKR measurements. The experimental measurements are taken in the Voigt geometry with the pumps being circularly polarized to generate spin polarization while the probe is linearly polarized to detect the spin dynamics (Fig. 1a). A lock-in detection scheme is employed to facilitate FRKR measurements.

For the double-pump single-probe scheme presented here, the incident beam from the source is split into three separate beams: Pump 1, Pump 2, and a probe beam (Fig. 1). Pump 1 and Pump 2 are first sent into two separate mechanical delay lines such that ΔT can be arbitrarily chosen. Arbitrarily choosing ΔT is of significant importance in the manipulation of RSA peaks, which will become apparent in the results section. The probe beam which is linearly polarized is sent into a mechanical chopper and modulated at 1370 Hz. After the pumps have generated the spin polarization, the incident probe is reflected off the sample and rotated by θ_k . This θ_k corresponds to the Kerr rotation and gives insight into the spin dynamics. The lock-in detection is used to read only the signal corresponding to the modulated frequency of the probe beam. See Ref. 9 for in-depth details regarding the pump-probe Kerr measurements.

The wavelength of interest for RSA corresponds to the resonance of the optical transition energy³. The active GaAs used in this model has a corresponding resonant wavelength of 818.8 nm and therefore the simulations and experimental results are all conducted at 818.8 nm. On resonance, the effects of the optical Stark effect and the resulting dynamic nuclear spin polarization can be neglected. Pump 2 has a static right circular polarization helicity and pump-probe delay ($\Delta t_2 = 13ns$) for all the measurements presented here because Pump 2 acts as the RSA generator. Furthermore, because Pump 1 acts as the RSA manipulator, the pump-probe

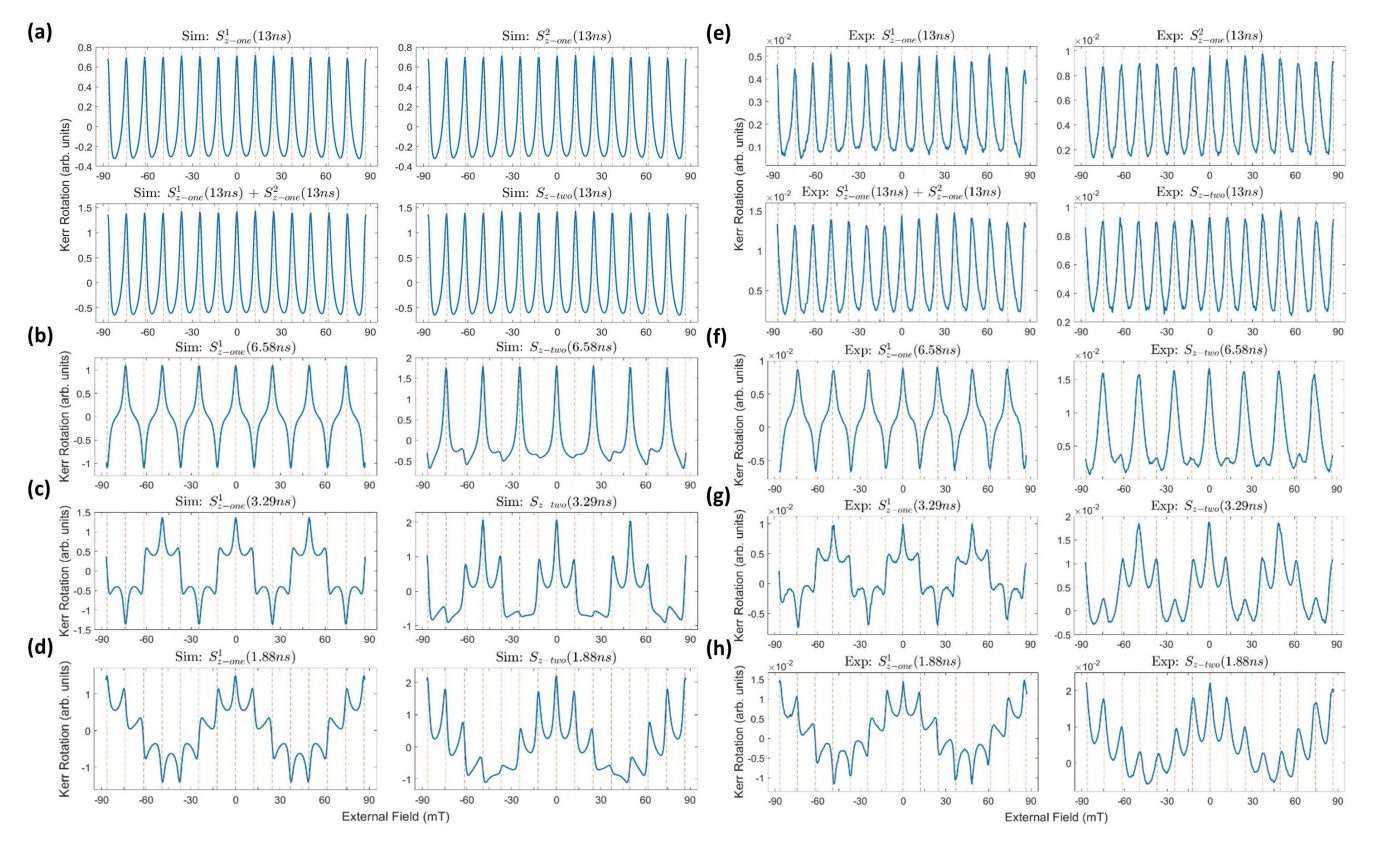


FIG. 3: RSA spectra for Pump 1 and Pump 2 having equal pump powers and the same polarization helicities. Pump 2 has a static pump-probe delay of 13 ns for all the results presented here. (a)–(d) Simulated RSA spectra. (e)–(h) Experimental RSA spectra. (a) & (e) Both pumps being superimposed and have a corresponding $\Delta T = T_{rep}$. (b) & (f) Pump 1 having a pump-probe delay of $T_{rep}/2$. (c) & (g) Pump 1 having a pump-probe delay of $T_{rep}/4$. (d) & (h) Pump 1 having a pump-probe delay of $T_{rep}/7$.

delay (Δt_1) and polarization helicity of Pump 1 is able to be put in any configuration to give the desired RSA spectra. For the field-dependent Kerr rotation measurement, ΔT is fixed and B_{ext} is swept in steps of 0.5 mT from -90 mT to 90 mT, then ΔT is changed from this set value by adjusting only Δt_1 while keeping Δt_2 fixed at 13 ns and B_{ext} is again swept from -90 mT to 90 mT. This is repeated for ΔT 's corresponding to 13.16 ns, 6.74 ns, 3.45 ns, and 2.04 ns where $\Delta T = \Delta t_1 + (T_{rep} - \Delta t_2)$. Additionally, the measurements are taken at each corresponding ΔT with Pump 1 and Pump 2 having the same and opposite polarization helicity. The above ΔT 's come from $\Delta t_1/\Delta t_2$ being equal to 13/13 ns, 6.58/13 ns, 3.29/13 ns, and 1.88/13 ns, respectively.

III. RESULTS

The vertical orange dashed lines in Fig. 3 and Fig. 4 correspond to the PSC which calls for ordinary RSA peaks every $B_n = n2\pi\hbar/\mu_B T_{rep}g$ where n is an integer. For this system, the sharp field-dependent peaks occur every integer multiple of ~12.3 mT. In the simulated and experimental RSA spectra, $S_{z-one}^1(\Delta t_1)/S_{z-one}^2(\Delta t_2)$ correspond to the z-component of the spin polarization for the system being in the single-pump single-probe regime obeying Eq. 9 while S_{z-two} corresponds to the z-component of the spin polarization for the system be-

ing in the double-pump single-probe regime obeying Eq. 11. The notation of the subscript z-one and z-two denotes the system being in the one-pump and two-pump regime, respectively. The superscript in S_{z-one} denotes which pump is being used in the one-pump regime. In other words, $S_{z-one}^1(\Delta t_1)$ will have the system in the one-pump regime with a corresponding pump-probe delay of Δt_1 , conversely, $S_{z-one}^2(\Delta t_2)$ will have the system in the one-pump regime with a corresponding pump-probe delay of Δt_2 . Pump 2 is the RSA generator and it is kept at a static pump-probe delay of 13 ns for all the spectra showcased here. Therefore, $S_{z-one}^2(13ns)$ has the same RSA spectra for all the cases presented hereafter and will only be explicitly shown for the case where both Pump 1 and Pump 2 have an equal pump-probe delay of 13 ns (Fig. 3a & 3e and Fig. 4a & 4e).

A. Pumps with Same Polarization Helicity

Ordinary RSA peaks in a one-pump model is necessary to comprehend in order to make sense of the consequences attributed to RSA when there are two pump pulses temporally separated from each other. In the two-pump model, when both pumps have the same pump powers, same polarization helicity, and $\Delta T = T_{rep}$, then $\overrightarrow{G} = \overrightarrow{G}'$ and $R(\Delta T - T_{rep}) = R(0) = 1$. This limiting case results in the two-pump regime trivially being equal to the one-pump regime with twice the generated

spin polarization (i.e., Eq. 11 equates to two times Eq. 9). Therefore, by configuring the two pumps to be RCP and setting $\Delta T = T_{rep}$, the two-pump regime is physically and mathematically equivalent to twice the one-pump regime and should result in ordinary RSA peaks found every integer multiple of \sim 12.3 mT with twofold the amplitude.

Fig. 3 shows the computational and experimental results where both Pump 1 and Pump 2 are RCP and have the same pump powers. The illustration where $\Delta T = T_{rep}$ and Eq. 11 simplifies to the one-pump regime with twice the amplitude is shown in Fig. 3a and Fig. 3e. Fig. 3a and Fig. 3e showcase ordinary RSA peaks for simulated and experimental results, respectively. The top left/right plots in Fig. 3a and Fig. 3e correspond to the z-components of the spin polarization generated from Pump 1/2 in the one-pump regime where both pump-probe delays (Δt_1 and Δt_2) are equal to 13 ns. The linear combination of S_{z-one}^1 and S_{z-one}^2 in the bottom left plots of Fig. 3a and Fig. 3e as well as the S_{z-two} in the bottom right plots of Fig. 3a and Fig. 3e verify that the resultant RSA peaks are twice the amplitude of the one-pump case.

Now, the ordinary RSA spectra is sustained by keeping Δt_2 at a constant pump-probe delay of 13 ns and the ordinary RSA spectra is then manipulated by varying Δt_1 . The left simulated/experimental RSA spectra in Fig. 3b/3f, Fig. 3c/3g, and Fig. 3d/3h represent different $S^1_{z-one}(\Delta t_1)$ with corresponding $\Delta t_1 = T_{rep}/2$, $T_{rep}/4$, and $T_{rep}/7$, respectively. Recall that $\Delta t_2 = 13$ ns for all the data presented here, and the resulting simulated/experimental RSA spectra are shown in Fig. 3a/3e. To mitigate redundancy, $S^2_{z-one}(\Delta t_2)$ RSA spectra have been omitted from Fig. 3b–3d and Fig. 3f–3h.

Letting $\Delta t_1 = T_{rep}/2$ in this system is approximately equivalent to having one pump pulse with a repetition period of $T_{rep}/2$. This can be better understood by observing $S_{\tau-one}^1(T_{rep}/2)$ shown in the left spectra in Fig. 3b (simulation) and Fig. 3f (experiment). The RSA peaks located every two times an integer multiple of the PSC destructively interfere with the ordinary RSA peaks. Therefore, when $\Delta t_1 = T_{rep}/2$, one would expect sharp field-dependent peaks with twice the period of the original system. In other words, for $\Delta t_1 = T_{rep}/2$, sharp field-dependent peaks should occur every \sim 24.6 mT rather than \sim 12.3 mT. This is computationally and experimentally verified for $S_{z-two}(T_{rep}/2)$ in the right spectra of Fig. 3b and Fig. 3f, respectively. When $\Delta t_1 = T_{rep}/n$ and n > 2, more interesting manipulations to the ordinary RSA peaks occur. Fig. 3c/3g and Fig. 3d/3h show the simulated/experimental results for $\Delta t_1 = T_{rep}/4$ and $T_{rep}/7$, respectively.

Looking at S_{z-two} in Fig. 3c/3g where $\Delta t_1 = T_{rep}/4$, there exists quenching of the RSA peaks at external fields matching the PSC that are not integer multiples of the denominator in Δt_1 , while the RSA peaks at integer multiples of the denominator in Δt_1 reach a maximum. Due to the consequent RSA peak quenching, the RSA spectra for $\Delta t_1 = T_{rep}/4$ follow a cosine beating envelope with a period of 4 times the ordinary PSC. This respective cosine beating envelope and its associated period is true for all $\Delta t_1 = T_{rep}/n$ where n > 2. In other words, the RSA spectra will carry a cosine beating envelope with a period of n times the PSC as long as $\Delta t_1 = T_{rep}/n$ and

n > 2. This is computationally/experimentally verified in Fig. 3c/3g and Fig. 3d/3h for $\Delta T = T_{rep}/4$ and $T_{rep}/7$, respectively.

B. Pumps with Opposite Polarization Helicity

Fig. 4 showcases the simulated and experimental results for both pumps having equal powers while Pump 1 and Pump 2 are LCP and RCP, respectively. The outcome of configuring the pumps to have opposite polarization helicities results in the spin generation vector having opposite signs for the corresponding pumps (i.e., $\overrightarrow{G} = -\overrightarrow{G}'$). Additionally, by setting $\Delta t_1 = \Delta t_2$ and configuring the pumps to have equal powers and opposite polarization helicities, then it is expected that S^1_{z-one} will have the same spectra as S^1_{z-two} with a change in sign (i.e., $S^1_{z-one} = -S^2_{z-one}$). The top left and top right spectra in Fig. 4a and Fig. 4e showcase simulation and experimental results that verify the preceding statement.

The spectra shown in Fig. 4a and Fig. 4e satisfy the condition $\Delta T = T_{rep}$ and $\overrightarrow{G} = -\overrightarrow{G}'$. These conditions give an equal amount of spin-up and spin-down filling in the conduction band. With this condition, it is expected that there will be no RSA because the difference between spin-up and spin-down excitations is zero. Plugging in $\Delta T = T_{rep}$ and $\overrightarrow{G} = -\overrightarrow{G}'$ into Eq. 11 agrees with this expectation and the corresponding simulated spectra in the bottom right plot of Fig. 4a shows no presence of RSA. However, achieving no RSA for these conditions in the two-pump model can be troublesome to carry out experimentally because of having to exactly match the Kerr rotation signal produced by each pump pulse.

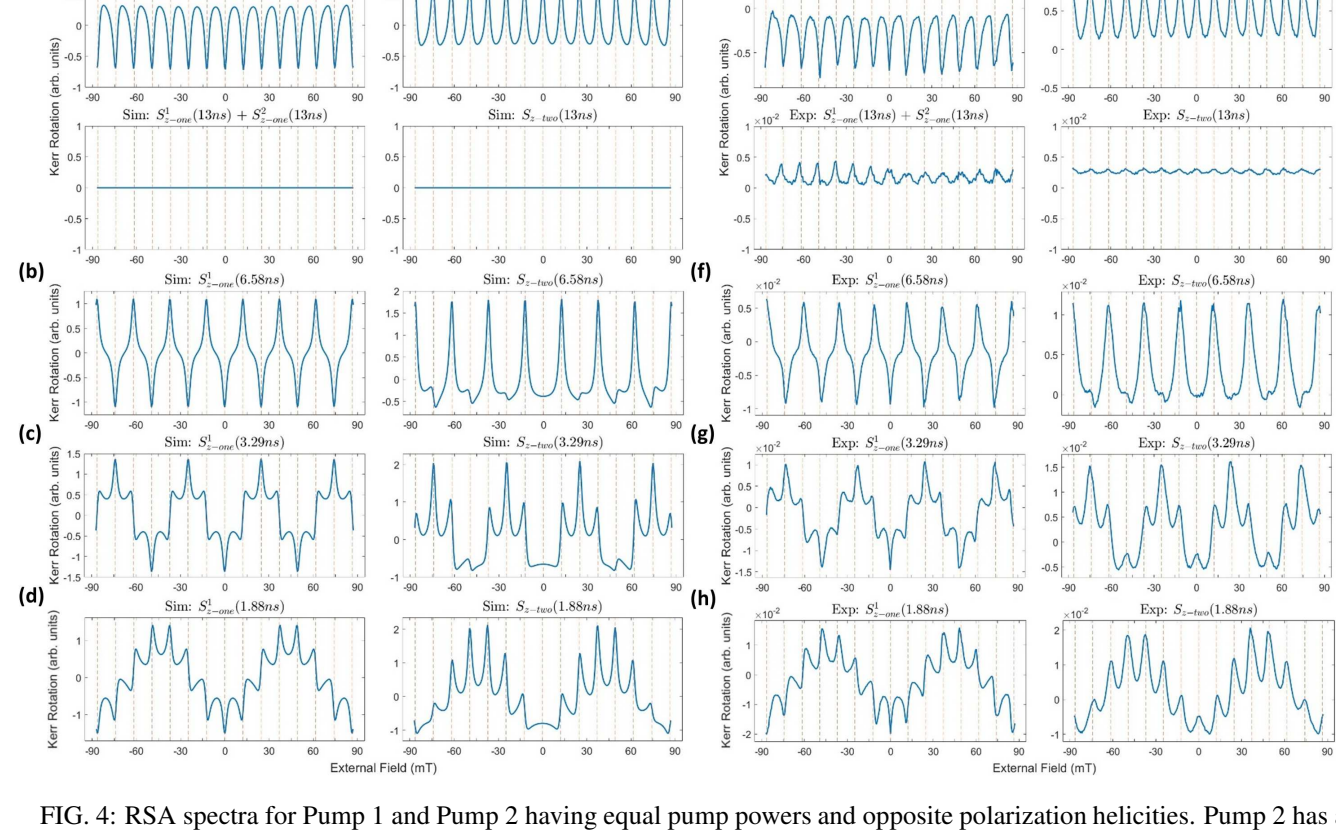
Small oscillations are present in the experimental results for the two-pump regime where $\Delta T = T_{rep}$ and $\overrightarrow{G} = -\overrightarrow{G}'$ (bottom right spectra of Fig. 4e). Comparing S^1_{z-one} and S^2_{z-one} in Fig. 4e show the generated RSA spectra from the individual pumps have the expected opposite signs but have unexpected differences in amplitude. This unexpected difference in amplitude can lead to the suspicion as to why there are small oscillations present in the experimental S_{z-two} in the bottom right spectra of Fig. 4e.

The spectra in Fig. 4e shows that S_{z-one}^2 has a slightly larger amplitude than S_{z-one}^1 which is also confirmed by S_{z-two} having maximum Kerr rotation aligning with the maximums of S_{z-one}^2 . Conversely, if S_{z-one}^1 had a larger amplitude than S_{z-one}^2 , then S_{z-two} would be expected to have minimum Kerr rotation aligning with the minimums of S_{z-one}^1 . If the pump powers, pump over lap, or pump beam spot sizes are not perfectly matched, then there will be a small difference of spin-up and spin-down filling in the conduction band. So, the small oscillations present in Fig. 4e are suspected to be from Pump 2 generating slightly more spin polarization than Pump 1. This could be a consequence of having the pump powers, pump overlap, or pump beam spot sizes not being perfectly matched.

Pump 2 generates only slightly more spin polarization than Pump 1, and this difference is less apparent in the data for the cases where $\Delta t_1 \neq \Delta t_2$ as presented in Fig. 4b–4d and Fig. 4f–4h. Following the same structure as Fig. 3, Δt_2 = 13 ns for all the results presented in Fig. 4, and the RSA spectra in Fig. 4b/4f, Fig. 4c/3g, and Fig. 4d/4h represent the

(a)

PLEASE CITE THIS ARTICLE AS DOI: 10.1063/5.0151281



(e)

FIG. 4: RSA spectra for Pump 1 and Pump 2 having equal pump powers and opposite polarization helicities. Pump 2 has a static pump-probe delay of 13 ns for all the results presented here. (a)–(d) Simulated RSA spectra. (e)–(h) Experimental RSA spectra. (a) & (e) Both pumps being superimposed and have a corresponding $\Delta T = T_{rep}$. (b) & (f) Pump 1 having a pump-probe delay of $T_{rep}/2$. (c) & (g) Pump 1 having a pump-probe delay of $T_{rep}/4$. (d) & (h) Pump 1 having a pump-probe delay of $T_{rep}/7$.

simulated/experimental results with the corresponding $\Delta t_1 = T_{rep}/2$, $T_{rep}/4$, and $T_{rep}/7$, respectively.

Similar to Fig. 3b and Fig. 3f, the field-dependent Kerr rotation presented in Fig. 4b and Fig. 4f for $\Delta t_1 = T_{rep}/2$ also has a period of 24.6 mT, but now the peaks are shifted along the x-axis by 12.3 mT. Notably, the RSA spectra still has twice the period of the RSA produced by a single pump pulse, but now has zero signal at zero external magnetic field. The shifting of the RSA spectra along the x-axis is also present for Δt_1 = $T_{rep}/4$ and $T_{rep}/7$, but with a corresponding x-axis shift of 24.6 mT and 43.05 mT, respectively. This shifting of the RSA spectra holds true for all $\Delta t_1 = T_{rep}/n$ and obeys PSC * n/2where n is the integer in the denominator of Δt_1 and the PSC is 12.3 mT for this system. Additionally, the quenching of subsequent RSA peaks still occur for $\Delta t_1 = T_{rep}/n$ and n > 2, but now the RSA spectra follow a sine beating envelope (Fig. 4c-4d and Fig. 4g-4h) instead of a cosine beating envelope (Fig. 3c-3d and Fig. 3g-3h) because of the x-axis shift of the respective RSA spectra.

IV. CONCLUSION

A computational and experimental optical pump train model with an infinite train of two pump pulses has been constructed to manipulate resonant spin amplification. The model takes one pump pulse to be the RSA generator (Pump 2) and the other pump pulse to be the RSA manipulator (Pump 1). Employing one pump to generate ordinary RSA spectra and another pump to manipulate the RSA spectra gives control in the selective generation of spin polarized electrons resulting in the RSA spectra no longer being entirely dependent on the externally applied magnetic field. The expected RSA spectra using this two pump model can be calculated for any given externally applied magnetic field, pump-pump temporal separation, pump-probe time delay, same or opposite pump polarization, and any combination of the mentioned degrees of freedom. The effects of RSA manipulation presented in this two-pump model can be used to conceptualize, characterize, and investigate models for RSA-based optospintronic devices.

ACKNOWLEDGEMENTS

E.K. gratefully acknowledges Dr. Hua-Wei Hsu for his thoughtful discussions regarding the experimental modeling. E.K. was supported by the University of Michigan's Rackham Science Fellowship. This material is based upon work supported by the National Science Foundation under Grant No. DMR-2207162. Sample fabrication was performed at the Lurie Nanofabrication Facility located at the University of Michigan.

Appendix A: Closed form solutions for $S_z(\Delta t)$

The closed form solutions for $S_{z-one}(\Delta t)$ and $S_{z-two}(\Delta t)$ used in this report were simplified using trigonometric and algebraic manipulations. The subscript convection z-one and

z-two denote the closed forms for the one- and two-pump models, respectively. Additionally, the spin generated from pump 1/2 ($\overrightarrow{G}'/\overrightarrow{G}$) is taken to be S'_0/S_0 where S'_0 and S_0 must follow the +/- sign convention for LCP/RCP.

$$S_{z-one}(\Delta t) = \frac{S_0 e^{\frac{T_{rep} - \Delta t}{T_2^*}} \left(\cos(\Omega \Delta t) e^{\frac{T_{rep}}{T_2^*}} - \cos(\Omega (T_{rep} - \Delta t)) \right)}{e^{\frac{2T_{rep}}{T_2^*}} - 2\cos(\Omega T_{rep}) e^{\frac{T_{rep}}{T_2^*}} + 1}$$
(A1)

$$S_{z-two}(\Delta t) = e^{\frac{T_{rep}-\Delta t}{T_{2}^{*}}} * \frac{\left(\cos(\Omega(\Delta t - \Delta T))S_{0}e^{\frac{\Delta T - T_{rep}}{T_{2}^{*}}} - \cos(\Omega(T_{rep} + \Delta t - \Delta T))S_{0}e^{\frac{\Delta T}{T_{2}^{*}}} + \cos(\Omega(T_{rep} - \Delta T))S'_{0} - \cos(\Omega\Delta t)S'_{0}e^{\frac{T_{rep}}{T_{2}^{*}}}\right)}{e^{\frac{2T_{rep}}{T_{2}^{*}}} - 2\cos(\Omega T_{rep})e^{\frac{T_{rep}}{T_{2}^{*}}} + 1}$$
(A2)

A clarification should be made here: the simulated RSA spectra for S_{z-two} can also be simulated by taking a linear combination of $S_{z-one}(\Delta t)$ at the two respective pump-probe time delays, i.e., taking $S_{z-two} = S_{z-one}(\Delta t_1) + S_{z-one}(\Delta t_2)$. However, the result of taking a linear combination of $S_{z-one}(\Delta t)$ at the two respective time delays to simulate the two-pump RSA spectra will not explicitly give an equation dependent on the temporal separations between the two pumps, which is shown in Fig. 1 as ΔT and $T_{rep} - \Delta T$.

The approach to take into account the temporal separations between the two pumps must invoke the relation $\overrightarrow{S}^+ = \overrightarrow{S}^-$. So, the first incident pump pulse at time t=0 generates \overrightarrow{G} , at the time of the second incident pump pulse $\overrightarrow{S}^- = \overrightarrow{S}(\Delta T)$, at the time of the third incident pump pulse $(t=T_{rep})$ $\overrightarrow{S}^- = \overrightarrow{S}(T_{rep} - \Delta T)$ and the resulting total spin vector after the three pump pulses is

$$S^{+}(T_{rep}) = R_{\Omega}(T_{rep} - \Delta T)R_{\Omega}(\Delta T)\overrightarrow{G}'e^{-T_{rep}/T_{2}^{*}} + R_{\Omega}(T_{rep} - \Delta T)\overrightarrow{G}e^{-(T_{rep} - \Delta T)/T_{2}^{*}} + \overrightarrow{G}'$$
(A3)

This process is repeated for an infinite train of the two pump pulses and the resulting $\overrightarrow{S}^+|_{\infty}$ becomes Eq. 11.

- ⁶I. A. Yugova, M. M. Glazov, D. R. Yakovlev, A. A. Sokolova, and M. Bayer, "Coherent spin dynamics of electrons and holes in semiconductor quantum wells and quantum dots under periodical optical excitation: Resonant spin amplification versus spin mode locking," Phys. Rev. B 85, 125304 (2012).
- ⁷S. Varwig, A. Schwan, D. Barmscheid, C. Müller, A. Greilich, I. A. Yugova, D. R. Yakovlev, D. Reuter, A. D. Wieck, and M. Bayer, "Hole spin precession in a (in,ga)as quantum dot ensemble: From resonant spin amplification to spin mode locking," Phys. Rev. B 86, 075321 (2012).
- ⁸J. Lohrenz, T. Paschen, and M. Betz, "Resonant spin amplification in intrinsic bulk germanium: Evidence for electron spin lifetimes exceeding 50 ns," Phys. Rev. B 89, 121201 (2014).
- ⁹M. Macmahon, J. R. Iafrate, M. J. Dominguez, and V. Sih, "Observation of magnetic field sweep direction dependent dynamic nuclear polarization under periodic optical electron spin pumping," Phys. Rev. B **99**, 075201 (2019).
- ¹⁰M. Luengo-Kovac, M. Macmahon, S. Huang, R. S. Goldman, and V. Sih, "g-factor modification in a bulk ingaas epilayer by an in-plane electric field," Phys. Rev. B 91, 201110 (2015).
- ¹¹M. J. Dominguez, J. R. Iafrate, and V. Sih, "Nuclear-induced frequency focusing and overhauser field distributions in periodically pumped gallium arsenide," Phys. Rev. B **104**, 235204 (2021).
- ¹²S. Markmann, C. Reichl, W. Wegscheider, and et al., "Universal nuclear focusing of confined electron spins," Nat Commun 10, 1097 (2019).
- ¹³E. A. Zhukov, O. A. Yugov, I. A. Yugova, D. R. Yakovlev, G. Karczewski, T. Wojtowicz, J. Kossut, and M. Bayer, "Resonant spin amplification of resident electrons in cdte/(cd,mg)te quantum wells subject to tilted magnetic fields," Phys. Rev. B 86, 245314 (2012).
- ¹⁴E. A. Zhukov, A. Greilich, D. R. Yakovlev, K. V. Kavokin, I. A. Yugova, O. A. Yugov, D. Suter, G. Karczewski, T. Wojtowicz, J. Kossut, V. V. Petrov, Y. K. Dolgikh, A. Pawlis, and M. Bayer, "All-optical nmr in semiconductors provided by resonant cooling of nuclear spins interacting with electrons in the resonant spin amplification regime," Phys. Rev. B 90, 085311 (2014).
- ¹⁵M. Kotur, F. Saeed, R. W. Mocek, V. L. Korenev, I. A. Akimov, A. S. Bhatti, D. R. Yakovlev, D. Suter, and M. Bayer, "Single-beam resonant spin amplification of electrons interacting with nuclei in a gaas/(al,ga)as quantum well," Phys. Rev. B 98, 205304 (2018).
- ¹⁶M. Griesbeck, M. M. Glazov, E. Y. Sherman, D. Schuh, W. Wegscheider, C. Schüller, and T. Korn, "Strongly anisotropic spin relaxation revealed by resonant spin amplification in (110) gaas quantum wells," Phys. Rev. B 85, 085313 (2012).
- ¹⁷S. Kuhlen, R. Ledesch, R. de Winter, M. Althammer, S. T. B. Gönnenwein, M. Opel, R. Gross, T. A. Wassner, M. S. Brandt, and B. Beschoten, "Unambiguous determination of spin dephas-

¹J. M. Kikkawa and D. D. Awschalom, "Resonant spin amplification in *n*-type gaas," Phys. Rev. Lett. **80**, 4313–4316 (1998).

²F. G. G. Hernandez, G. M. Gusev, and A. K. Bakarov, "Resonant optical control of the electrically induced spin polarization by periodic excitation," Phys. Rev. B 90, 041302 (2014).

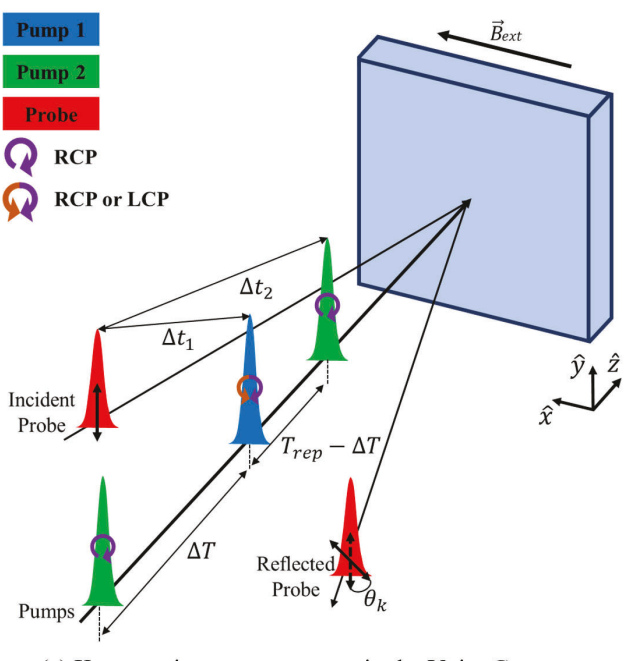
³M. J. Dominguez, J. R. Iafrate, and V. Sih, "Dynamic nuclear polarization by optical stark effect in periodically pumped gallium arsenide," Phys. Rev. B **101**, 205203 (2020).

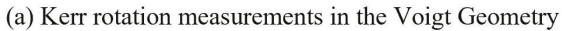
⁴I. Žutić, J. Fabian, and S. Das Sarma, "Spintronics: Fundamentals and applications," Rev. Mod. Phys. **76**, 323–410 (2004).

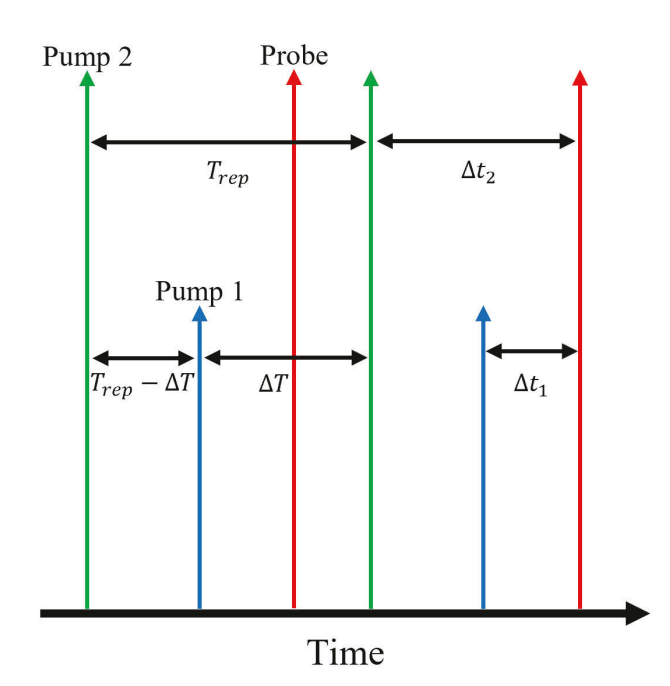
⁵ V. V. Belykh, D. N. Sob'yanin, and A. R. Korotneva, "Resonant spin amplification meets electron spin resonance in *n*-gaas," Phys. Rev. B **102**, 075201 (2020).

- ing times in zno by time-resolved magneto-optical pump-probe experiments," physica status solidi (b) **251**, 1861–1871 (2014), https://onlinelibrary.wiley.com/doi/pdf/10.1002/pssb.201350201.
- ¹⁸M. Glazov and E. Ivchenko, "Resonant spin amplification in nanostructures with anisotropic spin relaxation and spread of the electronic g factor," Semiconductors 42, 951957 (2008).
- ¹⁹M. Kugler, K. Korzekwa, P. Machnikowski, C. Gradl, S. Furthmeier, M. Griesbeck, M. Hirmer, D. Schuh, W. Wegscheider, T. Kuhn, C. Schüller, and T. Korn, "Decoherence-assisted initialization of a resident hole spin polarization in a *p*-doped semiconductor quantum well," Phys. Rev. B 84, 085327 (2011).
- ²⁰ A. Kolosvetov, M. Kozhaev, I. Savochkin, V. Belotelov, and A. Chernov, "Concept of the optomagnonic logic operation," Phys. Rev. Appl. 18, 054038 (2022).
- ²¹H. Shibata, M. Okano, and S. Watanabe, "Ultrafast control of coherent spin precession in ferromagnetic thin films via thermal spin excitation processes induced by two-pulse laser excitation," Phys. Rev. B 97, 014438 (2018).
- ²²E. A. Zhukov, D. R. Yakovlev, M. M. Glazov, L. Fokina, G. Karczewski, T. Wojtowicz, J. Kossut, and M. Bayer, "Optical control of electron spin coherence in cdte/(cd,mg)te quantum wells," Phys. Rev. B 81, 235320 (2010).
- ²³J. A. Gupta, R. Knobel, N. Samarth, and D. D. Awschalom, "Ultrafast manipulation of electron spin coherence," Science 292, 2458–2461 (2001),

- https://www.science.org/doi/pdf/10.1126/science.1061169.
- ²⁴J. Berezovsky, M. H. Mikkelsen, N. G. Stoltz, L. A. Coldren, and D. D. Awschalom, "Picosecond coherent optical manipulation of a single electron spin in a quantum dot," Science 320, 349–352 (2008), https://www.science.org/doi/pdf/10.1126/science.1154798.
- ²⁵ A. Greilich, S. Economou, S. Spatzek, and et al., "Ultrafast optical rotations of electron spins in quantum dots," Nature Phys 5, 262–266 (2009).
- ²⁶D. T. Pierce and F. Meier, "Photoemission of spin-polarized electrons from gaas," Phys. Rev. B 13, 5484–5500 (1976).
- ²⁷M. Dominguez, Analysis of the Coupled Electron and Nuclear Spin Systems from Optically Induced Dynamic Nuclear Polarization in GaAs, Ph.D. thesis, University of Michigan (2022).
- ²⁸C. J. Trowbridge and V. Sih, "Phase effects due to previous pulses in timeresolved faraday rotation measurements," Journal of Applied Physics 117, 063906 (2015), https://doi.org/10.1063/1.4907912.
- ²⁹M. Heidkamp, Spin-Coherence and -Dephasing of Donor and Free Conduction Band Electrons across the Metal-Insulator Transition in Si:GaAs, Ph.D. thesis, Technischen Hochschule Aachen (2004).
- ³⁰S. Varwig, I. A. Yugova, A. René, T. Kazimierczuk, A. Greilich, D. R. Yakovlev, D. Reuter, A. D. Wieck, and M. Bayer, "Excitation of complex spin dynamics patterns in a quantum-dot electron spin ensemble," Phys. Rev. B 90, 121301 (2014).







(b) Illustration of two pump model

